AIRS/Aqua Satellite Observations of Gravity Waves During the 2016 QBO Disruption

S. Kalisch[1] and H.-Y. Chun[1]

[1]Department of Atmospheric Sciences, Yonsei University, Seoul, South Kora

Corresponding author: Silvio Kalisch (s.kalisch@yonsei.ac.kr).

Key Points:

- Observed gravity waves during the disruption of the Quasi-biennial oscillation in 2015/2016
- AIRS/Aqua observed gravity wave activity prominent during QBO disruption
- Gravity wave activity higher in Pacific Ocean and South American region

Abstract

In early 2016 equatorward propagating extratropical Rossby waves caused a disruption of the quasi-biennial oscillation (QBO). In this study we show results from NASA's Atmospheric Infrared Sounder (AIRS) satellite instrument for our analysis. Variances in the 4.3μm CO_2 band brightness temperature are analysed. Spatial and temporal variations of gravity waves (GW) activity in the middle atmosphere are analysed for different regions in the tropics. Additionally, we use 8μm brightness temperature data from AIRS to control our findings for deep convective activity. Our results show an increase in GW variances during the QBO westerly phase prior the disruption with highest variances found in the pacific region. However, the Latin America region shows more prominent GW activity in January and February 2016. The temporal correlation of this increased GW activity with zonal winds were highest at the 30hPa level.

Plain Language Summary

The quasi-biennial-oscillation of the inner-tropical Stratosphere is a change in wind direction from eastward to westward with a period length of about 24 months. In 2016 this regular oscillation was suddenly interrupted. This interruption was caused by a combination of atmospheric waves including gravity waves. In this study we use satellite observation from NASA's Atmospheric Limb Sounder (AIRS) instrument to investigate the role of these gravity waves during the QBO disruption. Our results show particularly strong gravity wave activity over South America just prior the disruption and could explain why the disruption occurred.

1 Introduction

The quasi-biennial oscillation (QBO) is the descent of alternating easterly and westerly zonal winds in the equatorial stratosphere with a period of approximately 28 months (*Baldwin et al.*, 2001). Despite the QBO being limited to the inner tropical stratosphere, its impact ranges far into the extra-tropics and also into the troposphere. For instance, QBO modulation of tropical convection (*Lee et al.*, 2019; *Liess & Geller*, 2012; *Collimore et al.*, 2003), its influence on the Madden-Julian oscillation (*Yoo & Son*, 2016), the connection to the intensity of the polar vortex (*Anstey & Shepard*, 2014) and the impact on the growth and life-cycle of synoptic- and planetary-scale waves in the troposphere (*Garfinkel & Hartmann*, 2011) have been reported.

In early 2016, the descending QBO westerly phase was suddenly interrupted by easterly winds at an altitude of 40hPa. This event is the first occurrence of an interrupted QBO phase since the start of its observation in 1953 (*Osprey et al.*, 2016; *Newman et al.*, 2016). Further studies have shown that a major factor for the QBO disruption was the presence of equatorward-propagating extratropical Rossby waves, which were likely enhanced by the strong El Nino at the time (*Dunkerton*, 2016; *Coy et al.*, 2017). Furthermore, *Barton and McCormack* (2017) found that anomalous westerly winds in the subtropical lower stratosphere caused a refraction of the Rossby wave flux toward the equator.

According to theory, the QBO is maintained by selective filtering of vertically propagating equatorial planetary waves and gravity waves (*Holton & Lindzen*, 1972; *Lindzen & Holton*, 1968). Propagating waves break as they approach regions where the zonal wind of the background atmosphere matches the phases speed of the wave. As a result, the wave's momentum and energy are deposited. This "critical level" filtering explains the descent of the alternating wind regimes. Furthermore, one of the most prominent sources of GWs in the tropical stratosphere is deep convection (*Fritts & Alexander*, 2003; *Chun et al.*, 2004). The interaction between the stratospheric winds of the QBO and the upward propagating tropical gravity waves motivates this study.

2 Instrument and Data

2.1 The AIRS instrument

For this study we use data from the Atmospheric InfraRed Remote-Sensing (AIRS) instrument aboard NASA's Aqua satellite. Aqua was launched on May, 2nd 2002 from Vandenberg Air Force Base as the third satellite of the so-called A-Train satellite formation. The Aqua satellite operates in a nearly polar sun-synchronous orbit at about 705 km altitude with 100° inclination and an orbital period of 100 minutes. The AIRS instrument (*Aumann et al.*, 2003; *Aumann & Chahine et al.*, 2006) as one of the six instruments aboard Aqua started operation in May 2002. The observations provide nearly global coverage with 14.4 orbits per day. The measurements geometry ranges from nadir to sub-limb. The infrared radiance spectra of Earth's atmosphere are measured as across-track scan footprints and cover a ground distance of 1780 km. The diameter of the footprints is around 15 km at nadir separated by 18 km distance along the observation track. The spectral range of the AIRS measurements covers 3.74-15.4 µm in three spectral bands with a resolving power of $\lambda/\Delta\lambda$=1200.

2.2 The AIRS brightness temperature perturbation data

We analyzed measurements from multiple channels in the 4.3 µm spectral region. The activity of stratospheric GWs is inferred directly from AIRS radiance measurements following the approach of *Hoffmann et al.* (2010) (see also *Hoffmann et al.* (2013, 2014)). We analyze spectral mean brightness temperatures in the 4.3 µm CO_2 fundamental band (2322.5-2346.0 cm^{-1} and 2352.5-2367.0 cm^{-1}), which becomes optically thick in the mid-stratosphere. Background signals associated with large-scale temperature gradients or planetary waves are removed with the detrending procedure of *Wu et al.* (2004) (see also *Eckermann et al.*, 2006; *Alexander & Barnet*, 2007; *Hoffmann & Alexander*, 2010; *Hoffmann et al.*, 2014) The short wavelength limit of the observations is at approximately 30 km, based on Nyquist's theorem and a sampling distance of 14 km at nadir. The noise of the spectral mean brightness temperatures is approximately 0.059 K at a 250 K scene temperature (*Hoffmann et al.*, 2014). The 4.3 µm brightness temperature variances shown in this paper have been corrected for noise by subtracting noise variances scaled to the scene temperature. Additionally, we use the brightness

temperature at 8 µm as a proxy for tropical cloud top temperature to control the observed GW variances from the 4.3 µm channel for convective activity of the atmospheric background at its respective location.

2.3 The MERRA-2 reanalysis data set

We use reanalysis data from the Modern-Era Retrospective analysis for Research and Applications, Version 2 (MERRA-2) dataset (*Gelaro et al.,* 2017) for comparison with our satellite observations during the December 2015-May 2016 period. The MERRA-2 dataset provides zonal wind data (U) and geopotential height data (H) at 42 pressure levels from the surface up to 1 hPa altitude. For all calculations, we used the full resolution of MERRA-2 at 0.625° longitude and 0.5° latitude with a temporal resolution of 3 hours. For the purpose of this study output of the orographic and non-orographic GWD parameterizations is required. In MERRA-2, the parameterized GWD comprises the orographic GWD after *McFarlane* (1987) and the non-orographic GWD after *Garcia & Boville* (1994). Both parameterizations have been tuned to improve the seasonal transition of the southern polar night jet and to internally generate the quasi-biennial oscillation in the GEOS-5 (Goddard Earth Observing System) general circulation model, respectively (*Molod et al.,* 2012). The resulting GWD forcing is therefore the sum of the orographic and non-orographic GWD.

3 **Results**

Figure 1a shows brightness temperature perturbation (BTP) at the 4.3µm wavelength in blue averaged between 5°S and 5°N for May 2015-September 2016. The red line indicates the mean over the same period at approximately 0.0011 K. From November 2015 onward, an increase in BTP is noticeable and prevails until June 2016. This is more evident in Figure 1b which shows the variances of BTP over the same period. In particular, the steep increase in BTP variances from mid-December 2015 onward is exceptional. At its peak it reaches a maximum of 0.0023 K^2 in early January 2016 and stays at around 0.0020 K^2 until early March 2016. After this, variances decline to 0.0012 K^2 until May 2016. Additionally, an early phase of increasing

BTP variances is noticeable from about June 2015 till December 2015. In comparison, Figure 1c shows 5°S-5°N zonal wind data for 20 hPa, 30 hPa, and 40 hPa from the Merra-2 data set. Noticeable is the small minimum at 20 hPa altitude around January 1st, 2016. After this, zonal wind stabilizes around 10m/s (westerly) again. However, for 30 hPa, this inflection point is approached much later in early April 2016 with a minimum zonal wind speed of -6m/s (easterly). At 40 hPa altitude the wind direction progresses from 10m/s westerly to -17m/s and further below in easterly direction. It is noteworthy that the inflection of the 30 hPa zonal wind speed coincides with the end of the high BT variance data in Figure 1b (marked as a gray box). There appears to be a more fundamental relation between the 30 hPa zonal wind and GW activity here.

Although the 4.3µm data already show significant increase in general GW activity, the question arises how much of that activity stems from deep convection – the most prominent source of GWs in the inner tropics. For this we use 8µm brightness temperature data from AIRS which are sensitive to water vapor and provide temperature data from the top of the convective cloud. A higher temperature would therefore indicate a lower, less deep convective cloud, whereas low temperature indicates deep convection.

Figure 2a shows 8µm brightness temperature data for January 31st, 2016. Low brightness temperatures (blue colors) appear along the equator, the inter tropical convergence zone, and scattered over South America and the Atlantic Ocean. Mid- to higher latitudes also show lower temperatures. However, these stem most likely from the surface and occasional cirrus cloud activity. Most observed tropical temperatures are in the range higher than 280 K and indicate lower clouds or now clouds at all. Brightness temperatures lower than 280 K are much more scarce, thus, we chose 280 K as one threshold to distinguish between convection and non-convection. Furthermore, we introduce a 210 K, and a 250 K threshold for comparison. Figure 2b shows the number of events for the three different brightness temperature thresholds observed between 5°S and 5°N for the months December 2015, and January to March 2016. The blue bars show the results for the 280 K threshold, green bars for the 250 K threshold, and red bars for the 210 K threshold. The strict 210 K temperature threshold (red) shows as expected the fewest events with just below 200 consistently for all four months. The most events were counted for the higher temperature threshold of 280 K (blue) with counts between 7863 for December 2015 and 8763 for March 2016. For the 250 K threshold, values are around 2000 and also increasing through the four-month period. It is noteworthy that the observed increase in number of

convective events for the 280 K and 250 K threshold temperature is not seen in the 210 K case. This may indicate an increase in general convective activity with the exception of deep convection events.

This increase in general convection events (280 K threshold) is also exceptional in comparison to other QBO periods without disruption. Figure 2c shows the statistic for the 280 K during the December to March periods of 2002-2018. Each boxplot represents one respective month except for the 2015/2016 case which is indicated by a star. The orange line within the box indicates the median, the top and bottom of the box represent the standard deviation. Minima and maxima are shown as horizontal lines above and below the box. The median of all four months (orange lines) is found between 4000 and 6000 cases per month. The highest median cases are found for January conditions with a declining trend thereafter. Maxima of up to 6300 convective event are found for February conditions. The lowest amount of events is found for March with about 3600 events, and the spread between 25^{th} and 75^{th} percentile as indicated by the edges of the boxes is generally lower than 1500 events. However, the 2015/2016 events are significantly distinct with more than two times the events.

This raises the question about the geographical origin of these events. Are there any specific source regions? In order to answer that question, we subdivided the inner tropical region into 6 sub regions as shown as white boxes in Figure 3a. These regions are: The Pacific East (PE), South America (SA), Atlantic (At), Africa (Af), Indian Ocean (IO), and South East Asia (SEA). The yellow box (Ni) indicates the Nino3.4 region which we also included in our analysis. The data shown in Figure 3a is the variance of the 4.3µm wavelength brightness temperature in logarithmic scale for January 2016. High variances (orange-yellow) typically occur at 20°S during northern hemisphere summer season. The inner tropics however appear to have comparably low GW activity. Figures 3b show the time series of the 7 regions for the three different brightness temperature thresholds 280 K (blue), 250 K (red), and 210 K (black) during March 2015 till December 2016. In the Pacific East region, very strong GW activity from deep convection (210 K – black lines) is observed with variances up to $0.01K^2$ during December 2015. This feature appears also in the Nino3.4 region albeit with additional more GW activity from more shallow convection as indicated by the 250 K (red) and 280 K (blue) threshold data. Apparently, more GW variances originates from deep convection in the larger PE region compared to the smaller Nino3.4 region. In contrast, South America, the Atlantic, and Africa

show the opposite tendency with higher GW activity for more shallow convection. The Indian Ocean and South East Asia regions both show similar distinct peaks in variance for 210 K threshold temperature with up to 0.018K² during November 2015 to December 2015. Both regions also show increased GW activity for higher threshold temperatures. However, in February-March 2016 the SEA region also shows high GW activity with variances of up to 0.01K².

As mentioned before, the extra-tropical variances in the 4.3µm brightness temperature and therefore the GW activity is higher than in the inner tropics. Figures 3b (indicated with labels 'Tr') reflect that showing the results for a symmetric region spanning all longitudes. Generally, the 210 K threshold accounts for most of the variances in the inner tropics. The further the analysis region is expanded to the mid latitudes, the more prominent the variances become for 250 K and 280 K threshold temperature. Interestingly, for the 20°S-20°N (Tr20°) to 30°S-30°N (Tr30°) regions, highest variances of up to 0.03K² (Tr25° – black line) are found between December 2015 and March 2016. These exceptional high variances from shallow convection (250 K and 280 K) are also prominent in the extended Africa (Af20°) and South America (SA20°) regions. Both show variances exceeding 0.03K² for deep convection (210 K) during the December 2015-March 2016 period. For SA20° variances from 250 K and 280 K threshold temperature also exceed the 0.03K² limit. This includes also the Atlantic region (At20°), where variances over 0.02K² (250 K) are observed during December 2015. This is however not surprising since higher convective activity over the continents and subsequently higher convective GW activity is well known and has been investigated before (*Kalisch et al.*, 2016).

4 Summary and Conclusions

In this study we analyzed 4.3µm brightness temperature perturbation data from AIRS satellite observations during the period of the 2015/2016 QBO disruption and found increased variances in the inner tropical region. By further including 8µm brightness temperature data as a proxy for convection and subdividing the inner tropical region into 7 regions, we found increased GW activity from deep convection in the Pacific Ocean and South East Asian regions. In direct comparison the 210 K threshold for the 8µm BT data showed the largest variances in these regions, whilst over Africa and South America prominent variances were found for the 250 K and 280 K threshold temperatures. This implies that the larger pacific very deep convection was

the primary source of convective GW activity, whereas over the landmasses less deep convection was the main driver of convective GW activity. Furthermore, the inclusion of region further away from the equator showed far more prominent convective GW activity during the December 2015 to March 2016 period. Prominent peaks in the BT variances were found throughout all regions for the 210 K threshold temperature during November to December 2015 followed by increased GW activity for 250 K and 280 K BT threshold temperature. From these observations we may conclude that GW activity during the 2015/2016 QBO disruption was most prominent in the wider Pacific Ocean regions including the Nino3.4 sub-region. Furthermore, the prominent GW activity over the South American continent follows the increased general convection in that region. This has already been reported in other studies (*Geller et al.*, 2016). At first it was found that extratropical Rossby waves from the Northern Hemisphere disrupted the QBO (e.g. *Osprey* 2016). Additionally, equatorial wave flux was also found exceptionally strong. Prominent Mixed-Rossby-Gravity wave forcing and internal GW wave forcing weakened the western QBO phase during the early stage of the disruption. *Pahlavan et al.* (2021) found significant westwards forcing and prominent Rossby wave activity at 40hPa just before the QBO disruption. However, in February 2016, vertically propagating equatorial Rossby waves and small-scale convective GWs substantially decelerated the WQBO in addition to the extratropical Rossby waves (*Kang* 2020, 2022). However, since our analysis is based on observations alone, we may suggest further modeling studies to investigate the impact these convective GWs had during the 2015/2016 QBO disruption.

Acknowledgments, Samples, and Data

This work was supported by the National Research Foundation of Korea (NRF) grant funded by the South Korea government (MSIT) (2017R1A2B2008025).

The authors thank Lars Hoffmann for his helpful comments and advice.

Data Availability Statement

The AIRS temperature data can be downloaded from NASA's public data server at: https://airs.jpl.nasa.gov/data/get-data/standard-data/.

The AIRS brightness temperature perturbation data are available at: https://www.re3data.org/repository/r3d100012430.

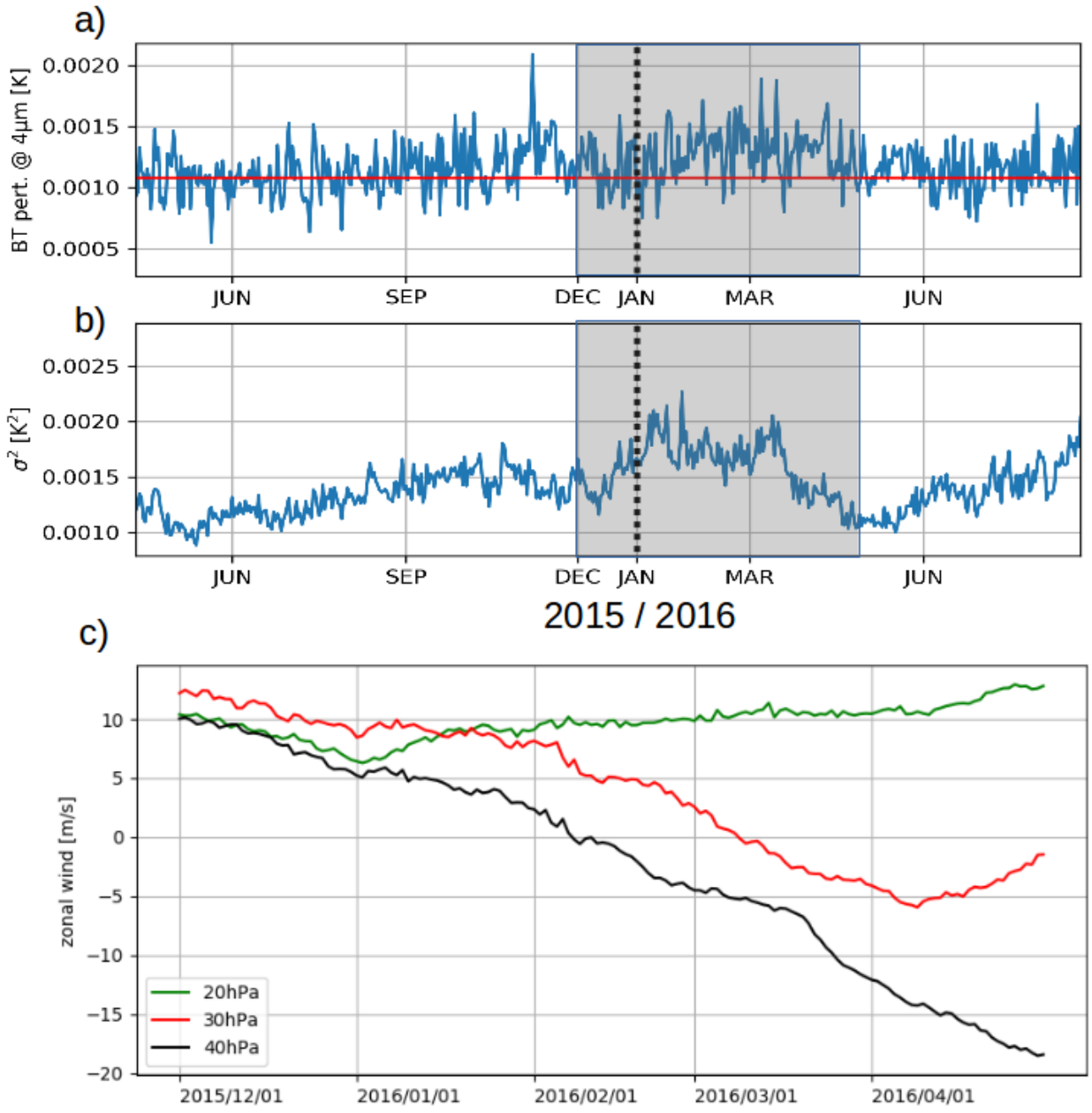

Figure 1: Brightness temperature perturbation from the 4.3um channel during 2015/2016 (panel a). Variances of BT perturbation data for the same period (panel b). Panel c shows Merra-2 zonal wind averaged between 5°S-5°N at 20hPa, 30hPa, and 40hPa altitude for December 2015-May 2016.

263

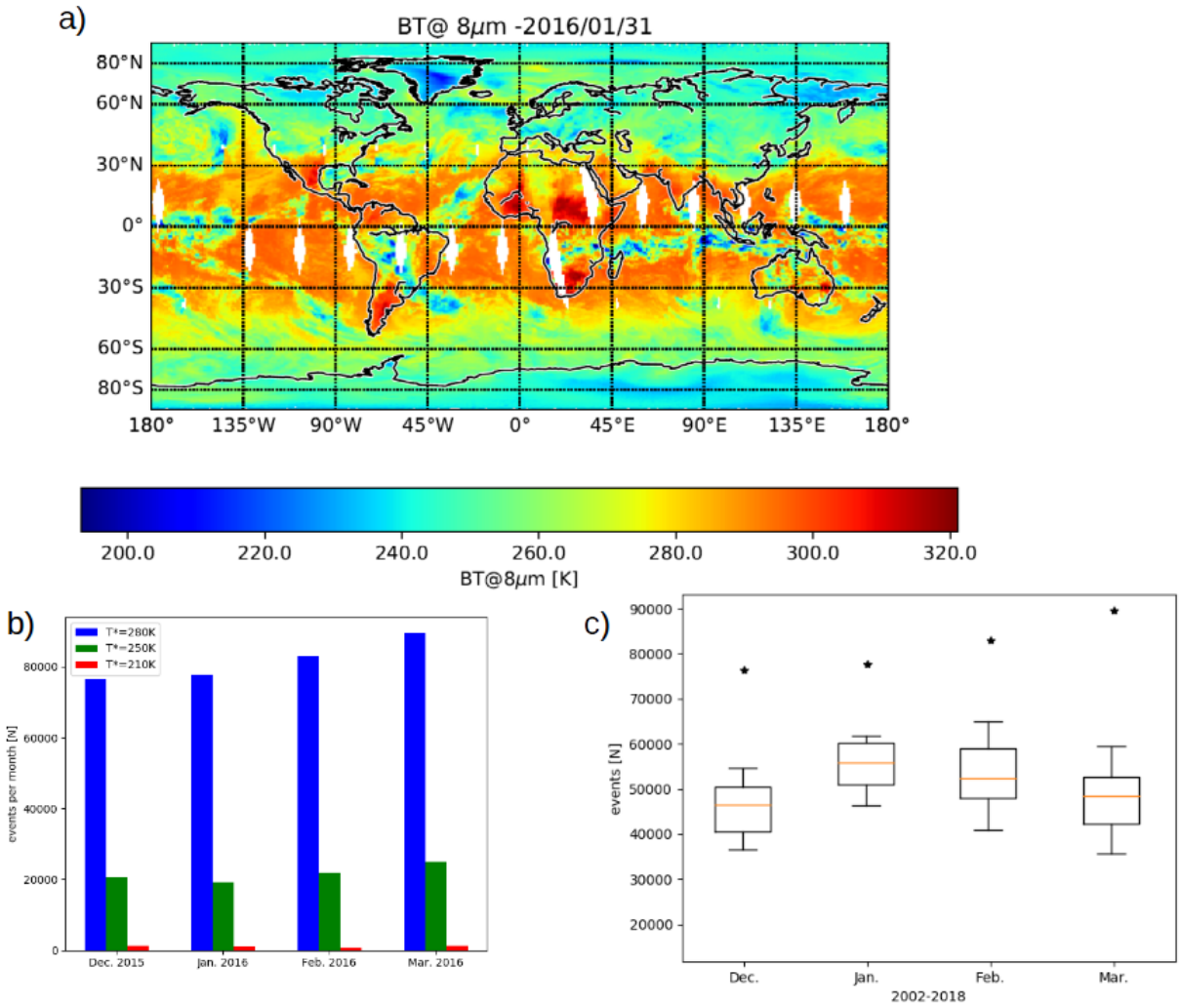

Figure 2: Brightness temperature at 8um wavelength for January 31st, 2016 (panel a). Panel b shows convective GW events for December 2015, and January-March 2016 for three different threshold temperature T - 280K (blue), 250K (green), and 210K (red). Panel c shows the statistic for the 2002-2020 climatology of the 280K threshold temperature. The 2015/2016 period is indicated by stars.*

264

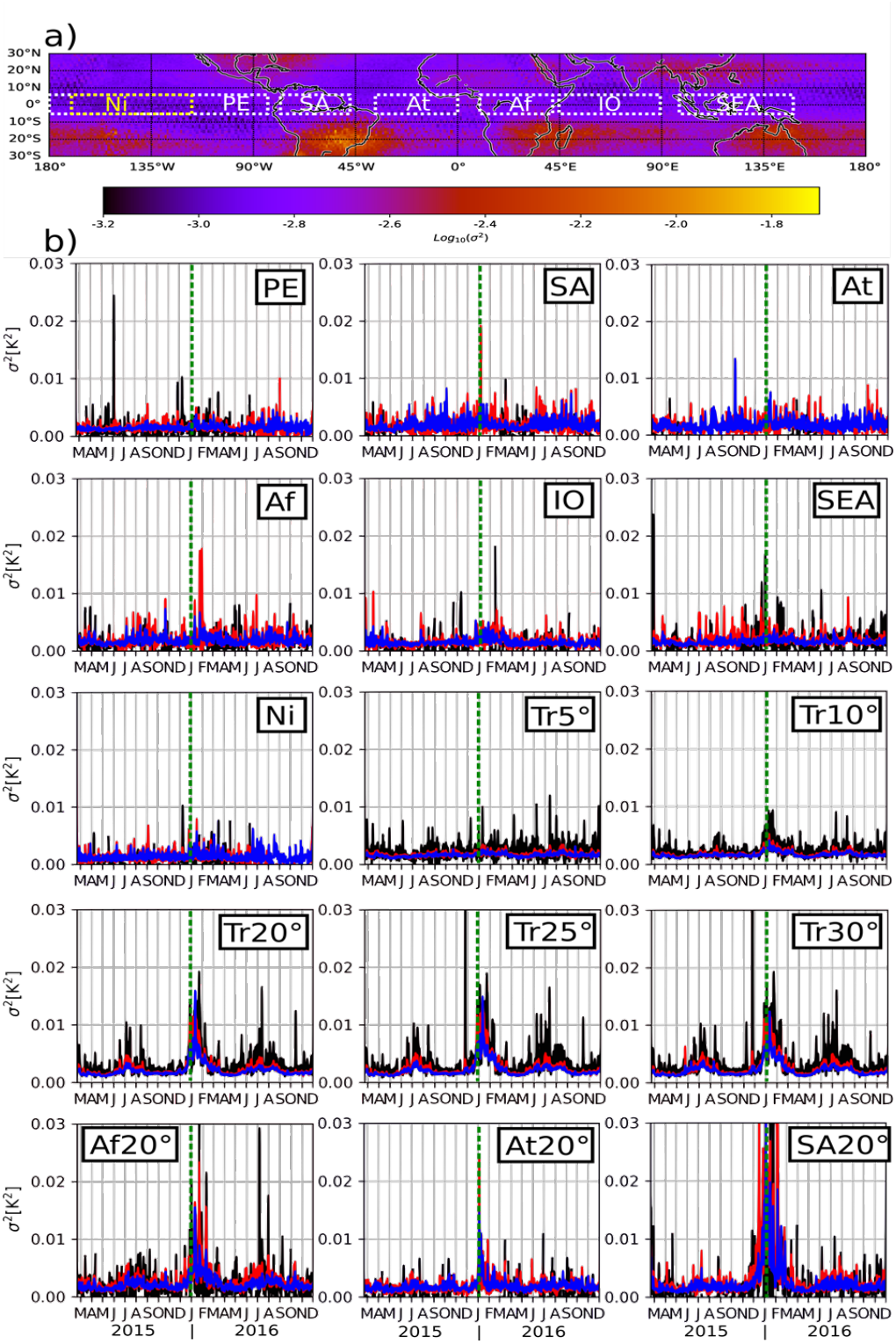

Figure 3: Variance of brightness temperature perturbation for January 2016 (panel a). Also indicated are the seven analysis regions. Panels b-p show variances of brightness temperature perturbations for 280K (blue), 250K (red), and 210K (black) threshold temperatures. Please refer to the text for more details.

References

Alexander, M. J. and Barnet, C. D.: Using satellite observations to constrain gravity wave parameterizations for global models, *J. Atmos. Sci.*, 64, 1652–1665, 2007

Anstey, J. A. and Shepherd, T. G.: High-latitude influence of the quasi-biennial oscillation, Q. J. *Roy. Meteorol. Soc.*, 140, 1–21, https://doi.org/10.1002/qj.2132, 2014

Aumann, H. H., Broberg, S., Elliott, D., Gaiser, S., & Gregorich, D. (2006). Three years of Atmospheric Infrared Sounder radiometric calibration validation using sea surface temperatures. *Journal of Geophysical Research*, 111(D16), D16S90. https://doi.org/10.1029/2005JD006822

Aumann, H. H., Chahine, M. T., Gautier, C., Goldberg, M. D., Kalnay, E., McMillin, L. M., et al. (2003). AIRS/AMSU/HSB on the Aqua mission: Design, science objective, data products, and processing systems. *IEEE Transactions on Geoscience and Remote Sensing*, 41,253–264.

Baldwin, M. P., Gray, L. J., Dunkerton, T. J., Hamilton, K., Haynes, P. H., Randel, W. J., et al. (2001). The quasi-biennial oscillation. *Reviews of Geophysics*, 39(2), 179–229. https://doi.org/10.1029/1999RG000073

Barton, C. A. and McCormack, J. P.: Origin of the 2016 QBO disruption and its relationship to extreme El Niño events, *Geophys. Res. Lett.*, 44, 11150–11157, https://doi.org/10.1002/2017GL075576, 2017

Chun, H. Y., Song, I. S., Baik, J. J., Kim, Y. J. (2004). Impact of a convectively forced gravity wave drag parameterization in NCAR CCM3. *Journal of Climate*, 17, 3530–3547. https://doi.org/10.1175/1520-0442(2004)017%3C3530:IOACFG%3E2.0.CO;2

Collimore, C. C., Martin, D. W., Hitchman, M. H., Huesmann, A., and Waliser, D. E.: On the relationship between the QBO and tropical deep convection, *Journal of Climate*, 16, 2552–2568, https://doi.org/10.1175/1520-0442(2003)016<2552:OTRBTQ>2.0.CO;2, 2003

Coy, L., Newman, P. A., Pawson, S., and Lait, L. R.: Dynamics of the disrupted 2015/16 quasi-biennial oscillation, *Journal of Climate*, 30, 5661–5674, https://doi.org/10.1175/JCLI-D-16-0663.1, 2017

Dunkerton, T. J.: The quasi-biennial oscillation of 2015–2016: Hiccup or death spiral?, *Geophys. Res. Lett.*, 43, 10547–10552, https://doi.org/10.1002/2016GL070921, 2016

Eckermann, S. D., Wu, D. L., Doyle, J. D., Burris, J. F., McGee, T. J., Hostetler, C. A., Coy, L., Lawrence, B. N., Stephens, A., McCormack, J. P., and Hogan, T. F.: Imaging gravity waves in lower stratospheric AMSU-A radiances, Part 2: Validation case study, Atmos. *Chem. Phys.*, 6, 3343–3362, doi:10.5194/acp-6-3343-2006, 2006.

Fritts, D. C., & Alexander, M. J. (2003). Gravity wave dynamics and effects in the middle atmosphere. *Reviews of Geophysics*, 41(1), 1003. https://doi.org/10.1029/2001RG000106

Garcia, R. R., & Boville, B. A, (1994). Downward control of the mean meridional circulation and temperature distribution of the polar winter stratosphere. *Journal of Geophysical Research*, 51, 2238–2245.

Garfinkel, C. I. and Hartmann, D. L.: The influence of the quasibiennial oscillation on the troposphere in wintertime in a hierarchy of models. Part I: Simplified dry GCMs, *J. Atmos. Sci.*, 68, 1273–1289, 2011

Gelaro, R., McCarty, W., Suárez, M. J., Todling, R., Molod, A., Takacs, L., et al. (2017). The modern-era retrospective analysis for research and applications, version 2 (MERRA-2). *Journal of Climate*, 30(14), 5419–5454. https://doi.org/10.1175/JCLI-D-16-0758.1

Geller, M. A., Zhou, T., and Yuan, W. (2016), The QBO, gravity waves forced by tropical convection, and ENSO, *J. Geophys. Res. Atmos.*, 121, 8886– 8895, doi:10.1002/2015JD024125

Gong, J., Wu, D. L., & Eckermann, S. D. (2012). Gravity wave variances and propagation derived from AIRS radiances. *Atmospheric Chemistry and Physics*, 12(4), 1701–1720. https://doi.org/10.5194/acp-12-1701-2012

Hoffmann, L., Alexander, M. J. (2010). Occurrence frequency of convective gravity waves during the North American thunderstorm season. *Journal of Geophysical Research*, 115(D20). https://doi.org/10.1029/2010JD014401

Hoffmann, L., Xue, X., Alexander, M. (2013). A global view of stratospheric gravity wave hotspots located with atmospheric infrared sounder observations. *Journal of Geophysical* Research: Atmospheres, 118(2), 416–434.

Hoffmann, L., Alexander, M. J., Clerbaux, C., Grimsdell, A. W., Meyer, C. I., Rößler, T., Tournier, B. (2014). Intercomparison of stratospheric gravity wave observations with AIRS and IASI. *Atmospheric Measurement Techniques*, 7(12), 4517–4537. https://doi.org/10.5194/amt-7-4517-2014

Holton, J. R., & Lindzen, R. S. (1972). An updated theory for the quasi-biennial cycle of the tropical stratosphere. *Journal of Atmospheric Sciences*, *29*(6), 1076-1080.

Kang, M. J., Chun, H. Y., Garcia, R. R. (2020). Role of equatorial waves and convective gravity waves in the 2015/16 quasi-biennial oscillation disruption. *Atmospheric Chemistry and Physics*, *20*(23), 14669-14693.

Kang, M. J., Chun, H. Y., Son, S. W., Garcia, R. R., An, S. I., Park, S. H. (2022). Role of tropical lower stratosphere winds in quasi-biennial oscillation disruptions. *Science Advances*, *8*(27), eabm7229.

Kalisch, S., Chun, H.-Y., Ern, M., Preusse, P., Trinh, Q., Eckermann, S., et al. (2016). Comparison of simulated and observed convective gravity waves. *Journal of Geophysical Research: Atmospheres*, 121(22), 13474–13492. https://doi.org/10.1002/2016JD025235

Lee, J.-H., Kang, M.-J., Chun, H.-Y.: Differences in the tropical convective activities at the opposite phases of the quasi-biennial oscillation, *Asia-Pac. J. Atmos. Sci.*, 55, 317–336, 2019

Lindzen, R. S., Holton, J. R. (1968). A theory of the quasi-biennial oscillation. *Journal of Atmospheric Sciences*, *25*(6), 1095-1107.

Liess, S. and Geller, M. A.: On the relationship between QBO and distribution of tropical deep convection, *J. Geophys. Res.*, 117, D03108, https://doi.org/10.1029/2011JD016317, 2012

McFarlane, N. A. (1987). The effect of orographically excited gravity wave drag on the general circulation of the lower stratosphere and troposphere. *Journal of Atmospheric Sciences*, *44*(14), 1775-1800.

Molod, A., Takacs, L., Suarez, M., Bacmeister, J., Song, I.-S., Eichmann, A. (2012). The GEOS-5 atmospheric general circulation model: Mean climate and development from MERRA to Fortuna. *In Technical Report Series on Global Modeling and Data Assimilation (Vol. 28).* Maryland: National Aeronautics and Space Administration (NASA), Goddard Space Flight Center Greenbelt.

Newman, P. A., Coy, L., Pawson, S., Lait, L. R.: The anomalous change in the QBO in 2015–2016, *Geophys. Res. Lett.*, 43, 8791–8797, https://doi.org/10.1002/2016GL070373, 2016

Osprey, S. M., Butchart, N., Knight, J. R., Scaife, A. A., Hamilton, K., Anstey, J. A., Schenzinger, V., Zhang, C.: An unexpected disruption of the atmospheric quasi-biennial oscillation, *Science*, 353, 1424–1427, https://doi.org/10.1126/science.aah4156, 2016

Pahlavan, H. A., Wallace, J. M., Fu, Q., & Kiladis, G. N. (2021). Revisiting the quasi-biennial oscillation as seen in ERA5. Part II: Evaluation of waves and wave forcing. *Journal of the Atmospheric Sciences*, *78*(3), 693-707.

Wu, D. L.: Mesoscale gravity wave variances from AMSU-A radiances, *Geophys. Res. Lett.*, 31, L12114, doi:10.1029/2004GL019562, 2004

Yoo, C., Son, S.-W.: Modulation of the boreal wintertime Madden-Julian oscillation by the stratospheric quasibiennial oscillation, *Geophys. Res. Lett.*, 43, 1392–1398, https://doi.org/10.1002/2016GL067762, 2016

Figure 1: Brightness temperature perturbation from the 4.3um channel during 2015/2016 (panel a). Variances of BT perturbation data for the same period (panel b). Panel c shows Merra-2 zonal wind averaged between 5°S-5°N at 20hPa, 30hPa, and 40hPa altitude for December 2015-May 2016.

Figure 2: Brightness temperature at 8um wavelength for January 31st, 2016 (panel a). Panel b shows convective GW events for December 2015, and January-March 2016 for three different threshold temperature T* - 280K (blue), 250K (green), and 210K (red). Panel c shows the statistic for the 2002-2020 climatology of the 280K threshold temperature. The 2015/2016 period is indicated by stars.

Figure 3: Variance of brightness temperature perturbation for January 2016 (panel a). Also indicated are the seven analysis regions. Panels b show variances of brightness temperature perturbations for 280K (blue), 250K (red), and 210K (black) threshold temperatures. Please refer to the text for more details.

362